Nonadiabatic wavepacket dynamics: *k*-space formulation

J. M. Pruneda[1,2] and Ivo Souza[1]
[1]*Department of Physics, University of California–Berkeley, Berkeley, California 94720, USA*
[2]*Centre d'Investigació en Nanociència i Nanotecnologia, (CSIC-ICN), Campus U.A.B., 08193 Bellaterra, Barcelona, Spain*
(Received 11 October 2008; revised manuscript received 8 December 2008; published 29 January 2009)

The time evolution of wavepackets in crystals in the presence of a homogeneous electric field is formulated in *k* space in a numerically tractable form. The dynamics is governed by separate equations for the motion of the wave form in *k* space and for the evolution of the underlying Bloch-type states. A one-dimensional tight-binding model is studied numerically and both Bloch oscillations and Zener tunneling are observed. The long-lived Bloch oscillations of the wavepacket center under weak fields are accompanied by oscillations in its spatial spread. These are analyzed in terms of a *k*-space expression for the spread having contributions from both the quantum metric and the Berry connection of the Bloch states. We find that when sizable spread oscillations do occur, they are mostly due to the latter term.

DOI: 10.1103/PhysRevB.79.045127 PACS number(s): 72.10.Bg, 78.20.Bh, 71.90.+q

I. INTRODUCTION

The study of the dynamics of electron wavepackets in crystals has experienced a revival in recent years. The development of heterostructure superlattices, photonic crystals, and optical lattices has opened new possibilities for the experimental realization of fundamental dynamical effects such as Bloch oscillations[1–5] and Zener tunneling.[6–8] The wavepacket picture of transport has also shed light on subtle transport phenomena in solids. For instance, the intrinsic anomalous Hall effect in ferromagnets was shown to result from a Berry-curvature term in the wavepacket group velocity.[9]

Numerical simulations provide valuable insights into the dynamics of wavepackets in crystals. For instance, Bouchard and Luban[10] carried out a detailed study on a one-dimensional biased lattice, finding a rich variety of dynamical phenomena (Bloch oscillations of the center of mass, coherent breathing modes, Zener tunneling, and intrawell oscillations) as a function of the field-free band structure, field strength, and the form of the initial wavepacket. In order to solve numerically the time-dependent Schrödinger equation, they employed a supercell geometry with hard-wall boundary conditions; care had to be taken to ensure that the wavepacket never came close to the hard-wall boundaries for the duration of the simulation. In situations where unbounded acceleration (via Zener tunneling) of a significant portion of the wavepacket takes place, a large supercell must then be used, which may become computationally demanding. In principle that can be avoided by switching from hard-wall to periodic boundary conditions. However, the inclusion in the Hamiltonian of the nonperiodic electric-field term $e\mathcal{E}\cdot\mathbf{r}$ then becomes problematic. A successful numerical strategy for describing homogeneous electric fields under periodic boundary conditions was developed in Refs. 11 and 12 for static fields and generalized to time-dependent fields in Ref. 13.

In Refs. 11–13 the goal was to solve for the electronic structure of insulators in the presence of a homogeneous field. In this work we use a similar strategy to describe wavepacket dynamics. Our starting point is to express the wavepacket as a linear superposition of Bloch states,

$$|\phi\rangle = \int_0^{2\pi/a} dk f_k |\psi_k\rangle = \int_0^{2\pi/a} dk e^{ikx} f_k |v_k\rangle \tag{1}$$

(for simplicity we shall work in one dimension), and to follow the time evolution of both the wave form f_k and the underlying states $|v_k\rangle$. If a wavepacket—initially prepared in a given band—is constrained to remain in the same band at later times, one obtains the "semiclassical" approximation, which becomes exact in the adiabatic limit. Instead, we will allow for a fully unconstrained time evolution. As a result, for $t>0$ the states $|\psi_k\rangle$ may become an admixture $\Sigma_n c_{nk}|\psi^{(0)}_{nk}\rangle$ of several eigenstates of the crystal Hamiltonian H^0. We shall refer to such nonadiabatic states as Bloch-type, since they retain the Bloch form, with $v_k(x+a)=v_k(x)$.

Equation (1) is closely related to the crystal-momentum representation (CMR) of $|\phi\rangle$.[14,15] In the CMR the wavepacket is expressed in terms of the field-free Bloch eigenstates, with expansion coefficients $f_k c_{nk}$. Instead, the expansion (1) is in terms of the field-polarized states $|\psi_k\rangle$, whose time evolution must then be determined alongside that of f_k. Compared to the CMR approach, we have replaced having to solve for the complete set of eigenstates $|\psi^{(0)}_{nk}\rangle$ with having to solve for a single state $|\psi_k\rangle$ at each k and every time step.

The paper is organized as follows. The equations of motion for f_k and $|v_k\rangle$ and the expressions for the center and spread of the packet in terms of them are derived in Secs. II and III, respectively. In Sec. IV we perform simulations for a one-dimensional tight-binding Hamiltonian, using a numerically tractable form—given in the Appendix—of those equations.

II. DYNAMICAL EQUATIONS IN *k* SPACE

The wavepacket evolves according to the Schrödinger equation ($e=\hbar=1$),

$$i\frac{d|\phi\rangle}{dt} = (H^0 + \mathcal{E}x)|\phi\rangle, \tag{2}$$

where $\mathcal{E}$ is the electric field, which can be time-dependent but must be spatially uniform. Since f_k and $|v_k\rangle$ enter Eq. (1)

as a product, they are individually defined only up to a multiplicative factor which—because $\langle v_k|v_k\rangle=1$—must take the form $e^{i\varphi_k}$. We fix this phase arbitrariness by choosing f_k to be real and positive.

Inserting Eq. (1) into Eq. (2),

$$i\int dke^{ikx}(f_k|\dot{v}_k\rangle+\dot{f}_k|v_k\rangle) = \int dke^{ikx}H_k^0 f_k|v_k\rangle+\mathcal{E}\int dke^{ikx}xf_k|v_k\rangle, \tag{3}$$

where $H_k^0=e^{-ikx}H^0e^{ikx}$ and henceforth the integration range from 0 to $2\pi/a$ will be implied. Rewriting

$$\mathcal{E}\int dk(-i\partial_k e^{ikx})f_k|v_k\rangle=\mathcal{E}\int dke^{ikx}i(|v_k\rangle\partial_k f_k+f_k|\partial_k v_k\rangle) \tag{4}$$

($\partial_k\equiv\partial/\partial k$ and an integration by parts was performed) then yields, at each k,

$$if_k|\dot{v}_k\rangle+i\dot{f}_k|v_k\rangle=H_k^0f_k|v_k\rangle+i\mathcal{E}(|v_k\rangle\partial_k f_k+f_k|\partial_k v_k\rangle). \tag{5}$$

Contracting with $\langle v_k|$ and subtracting from the resulting equation its complex conjugate, we arrive at the equation of motion for f_k,

$$\dot{f}_k=\mathcal{E}\partial_k f_k, \tag{6}$$

where the reality of f_k was used, together with the relations $\langle\dot{v}_k|v_k\rangle=-\langle v_k|\dot{v}_k\rangle$ and $\langle\partial_k v_k|v_k\rangle=-\langle v_k|\partial_k v_k\rangle$. To find the equation of motion for $|v_k\rangle$ we plug Eq. (6) back into Eq. (5),

$$i|\dot{v}_k\rangle=(H_k^0+i\mathcal{E}\partial_k)|v_k\rangle. \tag{7}$$

Equations (6) and (7) govern the coherent wavepacket dynamics. Equation (7) was previously obtained in Ref. 13, where it was shown to describe the dynamics of valence electrons in insulators under the homogeneous field $\mathcal{E}(t)$. Here it describes the nonadiabatic evolution of the Bloch-type states $|v_k\rangle$ supporting the wavepacket.

As for Eq. (6), it determines the k-space dynamics of the wave form. In particular, it leads[15] to the familiar expression $\langle k\rangle_t=\langle k\rangle_0-\mathcal{E}t$ for the time evolution of the k-space center of the packet; a result which remains valid in the presence of interband mixing (Ref. 16, Appendix E). It is easily seen that the dynamical equation for f_k^2 is the same as that for f_k, namely, $df_k^2/dt=\mathcal{E}\partial_k f_k^2$. In this form Eq. (6) was derived in Ref. 15, working in the CMR.[17] Finally, we note that in spite of being reminiscent of the collisionless Boltzmann equation,[15,16] the meaning of Eq. (6) is quite distinct: while the Boltzmann equation deals with the time evolution of the distribution of carriers in phase space, Eq. (6) deals with the coherent time evolution of a single carrier (wavepacket) having a finite extent in k space.

For numerical implementation, the k derivatives must be replaced by finite-difference expressions over a k-point mesh. While such discretization is straightforward for Eq. (6), Eq. (7) requires some care. As in Ref. 13, we replace it with

$$i|\dot{v}'_k\rangle=(H_k^0+i\mathcal{E}\tilde{\partial}_k)|v'_k\rangle, \tag{8}$$

where $|\tilde{\partial}_k v'_k\rangle\equiv Q_k|\partial_k v'_k\rangle$ $(Q_k=1-|v_k\rangle\langle v_k|=1-P_k)$. Unlike $|\partial_k v_k\rangle$, $|\tilde{\partial}_k v'_k\rangle$ lends itself to a numerically robust finite-differences representation (see the Appendix).

The states $|v'_k\rangle$ obeying Eq. (8) differ from the states $|v_k\rangle$ in Eq. (7) by a phase factor,

$$|v'_k\rangle=e^{i\beta_k}|v_k\rangle=U_k|v_k\rangle, \tag{9}$$

which we must keep track of. Inserting Eq. (9) into Eq. (8) and using Eq. (7) yields

$$i\dot{U}_k=-\mathcal{E}A_kU_k, \tag{10}$$

where A_k is the Berry connection,

$$A_k=i\langle v_k|\partial_k v_k\rangle. \tag{11}$$

Equations (6), (8), and (10) are the desired dynamical equations for f_k, $|v'_k\rangle$, and U_k. Together they determine the time evolution of the wavepacket,

$$|\phi\rangle=\int dk\ f_ke^{ikx}U_k^*|v'_k\rangle. \tag{12}$$

In practice Eqs. (8) and (11) are replaced by the discretized forms (A3) and (A6), respectively.

III. WAVEPACKET CENTER AND SPREAD

In Sec. II we formulated the dynamics of the wavepacket (1) in terms of f_k and $|v_k\rangle$. Here we shall express its center and spread in terms of those same k-space quantities.

A. k-space expressions

Let us define the generating function for the spatial distribution of the wavepacket,

$$C(q)=\langle\phi|e^{-iqx}|\phi\rangle=\frac{2\pi}{a}\int dk\ f_kf_{k+q}\langle v_k|v_{k+q}\rangle, \tag{13}$$

where the second equality follows from Eq. (1) together with the identity,

$$\langle\psi_{k_1}|e^{-iqx}|\psi_{k_2}\rangle=\frac{2\pi}{a}\delta(k_2-k_1-q)\langle v_{k_1}|v_{k_1+q}\rangle. \tag{14}$$

The first moment is given by

$$\langle x\rangle=i\partial_qC(q)|_{q=0}=\langle iD_k\rangle=\langle A_k\rangle, \tag{15}$$

where iD_k is the Hermitian operator,

$$iD_k=i\partial_k+A_k, \tag{16}$$

and we have introduced the notation

$$\langle\mathcal{O}_k\rangle\equiv\frac{2\pi}{a}\int dkf_k\mathcal{O}_kf_k. \tag{17}$$

The last equality in Eq. (15) follows from f_k being real.

Next we evaluate the spread,

$$(\Delta x)^2 = \langle x^2\rangle - \langle x\rangle^2. \tag{18}$$

For $\langle x\rangle^2$ we use Eq. (15), while $\langle x^2\rangle$ is given by $i^2\partial_q^2 C(q)|_{q=0}$,

$$\langle x^2\rangle = \frac{2\pi}{a}\left[\int dk(\partial_k f_k)^2 + \int dk\ f_k^2\langle\partial_k v_k|\partial_k v_k\rangle\right]. \tag{19}$$

Inserting $1=P_k+Q_k$ in the last term on the right-hand side (RHS) and then combining with Eq. (15) yields

$$(\Delta x)^2 = \frac{2\pi}{a}\int dk(\partial_k f_k)^2 + \langle G_k\rangle + \langle(\Delta A_k)^2\rangle, \tag{20}$$

where G_k is the quantum metric,[18]

$$G_k = \langle\tilde{\partial}_k v_k|\tilde{\partial}_k v_k\rangle. \tag{21}$$

All three terms in Eq. (20) are manifestly non-negative. The first one only depends on f_k, while the remaining two also depend on the states $|v_k\rangle$. However, the second term is insensitive to the phases of those states [it is invariant under the gauge transformation (A9)], whereas the third term is phase dependent.

It is instructive to consider the limit of a uniform wave form $f_k=a/2\pi$, in which $|\phi\rangle$ becomes a Wannier function. Equation (15) can then be recast as $\langle x\rangle=a\varphi/2\pi$, where $\varphi=\int dk\ A_k$ is the Berry phase associated with the manifold of states $|v_k\rangle$.[19] The first term on the RHS of Eq. (20) then vanishes identically, while the second and third terms reduce to the gauge-invariant and gauge-dependent parts of the Wannier spread for an isolated band in one dimension, given, respectively, by Eqs. (C12) and (C17) of Ref. 18.

B. Uncertainty relation and minimal wavepackets

An alternative decomposition of the wavepacket spread may be obtained by noting that

$$\langle(iD_k)^2\rangle = \frac{2\pi}{a}\int dk(\partial_k f_k)^2 + \langle A_k^2\rangle, \tag{22}$$

as can be readily verified using the hermiticity of iD_k and the reality of f_k. Comparison with Eqs. (15) and (20) shows that

$$(\Delta x)^2 = \langle[\Delta(iD_k)]^2\rangle + \langle G_k\rangle. \tag{23}$$

Combining this with the relation

$$(\Delta A)^2(\Delta B)^2 \geq \frac{1}{4}|\langle[A,B]\rangle|^2 \tag{24}$$

yields, upon setting $A=iD_k$, $B=k$, and using $[iD_k,k]=i$,

$$[(\Delta x)^2 - \langle G_k\rangle](\Delta k)^2 \geq \frac{1}{4}. \tag{25}$$

In the limit of a vanishing lattice potential $G_k\to 0$ and $k\to p$ (canonical momentum). Equation (25) then reduces the familiar Heisenberg uncertainty relation.

Let us now show that Eq. (25) becomes an equality for minimal wavepackets in one dimension. Once the manifold of states $|v_k\rangle$ and the width Δk of the wave form are specified, all that remains is to set the phases of the $|v_k\rangle$ and the shape of f_k. We wish to minimize the spread (20) with respect to those two parameters. We start with the phases, which only affect the term $\langle(\Delta A_k)^2\rangle$. This term vanishes when A_k is constant,[20] in which case

$$(\Delta x)^2 - \langle G_k\rangle = \frac{2\pi}{a}\int dk(\partial_k f_k)^2. \tag{26}$$

Combining the previous two equations,

$$\frac{2\pi}{a}\int dk(\partial_k f_k)^2 \geq \frac{1}{4(\Delta k)^2}. \tag{27}$$

It can be verified that for $\Delta k \ll 2\pi/a$ this becomes an equality when the wave form has a Gaussian shape. In conclusion, a minimal wavepacket in one dimension is characterized by a Gaussian-shaped f_k and a constant Berry connection A_k in the region of k space where f_k is non-negligible. Its spread equals

$$(\Delta x)^2_{\min} = \frac{1}{4(\Delta k)^2} + \langle G_k\rangle. \tag{28}$$

It was shown in Ref. 18 that the spread of a maximally localized Wannier function in one dimension is $(\Delta x)^2_{\min}=\langle G_k\rangle$. This result can be viewed as the limit $\Delta k\to\infty$ of Eq. (28). In the opposite limit of a narrow wave form, the wavepacket spread becomes dominated by the term $1/4(\Delta k)^2$, as will be illustrated in Sec. IV B.

IV. NUMERICAL RESULTS

A. Tight-binding model

We have applied our scheme to the same one-dimensional tight-binding model used in Ref. 13. This is a three-band Hamiltonian with three atoms per unit cell of length $a=1$ and one orbital per atom,

$$H^0 = \sum_j\{\epsilon_j c_j^\dagger c_j + \gamma[c_j^\dagger c_{j+1} + c_{j+1}^\dagger c_j]\}, \tag{29}$$

with the site energy given by $\epsilon_{3m+l}=U\cos\beta_l$. Here m is the cell index, $l=\{-1,0,1\}$ is the site index, and $\beta_l=2\pi l/3$. The upper panel of Fig. 1 shows the energy dispersion for $\gamma=-U=1$.

Before the spatial distribution of the wavepacket can be defined, the matrix elements of the position operator must be specified. As in Ref. 13 we choose the simplest diagonal representation $x=\Sigma_j x_j c_j^\dagger c_j$, with $x_j=j/3$. The lower panel of Fig. 1 shows the quantum metric calculated for the Bloch states in the lowest band. As expected from the relation[21] $G_k\leq 1/2E_g^{(k)}$ ($E_g^{(k)}$ is the direct gap to the second band), G_k peaks around $k=0$.

We will now study numerically the wavepacket dynamics on this model. In Secs. IV B and IV C we consider, respectively, Bloch oscillations in a weak field and Zener tunneling in a strong field. In both cases we gradually turn on the field over a time interval T, as $\mathcal{E}(t)=\mathcal{E}_0\sin(\pi t/2T)$, and keep it constant after. The simulations begin with a minimal wavepacket prepared in the lowest band. Unless otherwise noted, the width of the Gaussian wave form is $\Delta k=0.075\times 2\pi$.

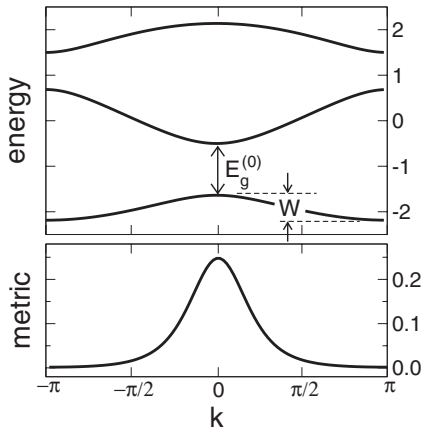

FIG. 1. Upper panel: band structure of the one-dimensional tight-binding model of Eq. (29), for the choice of parameters $\gamma=-U=1$. Lower panel: quantum metric [Eq. (21)] for the lowest band.

B. Bloch oscillations in a weak electric field

In order to observe long-lived Bloch oscillations we choose a weak field $\mathcal{E}_0=0.055\ll E_g^{(0)}/a$, which we turn on over a time interval of the order of the Bloch oscillation period $\tau_B=2\pi/\mathcal{E}_0 a$ (henceforth in this section, we choose $t=0$ long after the field has saturated at $\mathcal{E}_0$). 100 k points are used to sample the Brillouin zone and the time step is $\Delta t=1.7\times10^{-5}\tau_B$.

In the upper panel of Fig. 2 the weights $|\langle j|\phi\rangle|^2$ of the wavepacket on the tight-binding orbitals $|j\rangle$ are used to depict its spatial distribution as a function of time. The Bloch oscillations of $\langle x\rangle$ are clearly seen. In the lower panel we plot the oscillation amplitude A versus the width W of the lowest band, which was tuned by adjusting the tight-binding parameters in the range $0.5\leq\gamma\leq1.5$ and $-1.5\leq U\leq-0.5$. A and W are linearly related, with a slope $A/W\simeq8.5$. This is in agreement with the prediction $A=(1/2)(W/\mathcal{E}_0)|S_0|$ valid for a single-band tight-binding model.[10] The dimensionless parameter S_0 depends on the initial choice of wavepacket, but its magnitude cannot exceed unity; in the present case $1/2\mathcal{E}_0\simeq9.09$, so that $|S_0|\simeq0.9$.

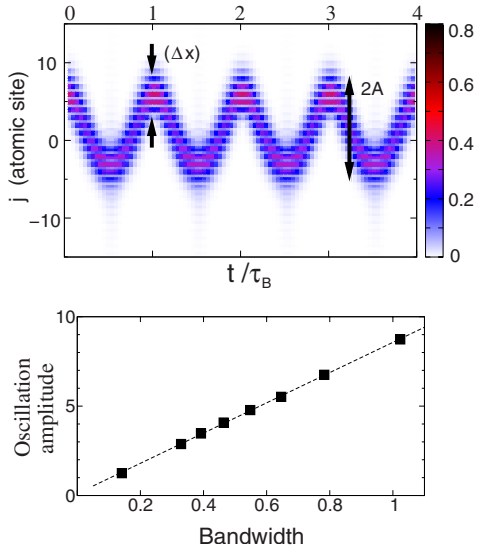

FIG. 2. (Color online) Bloch oscillations of a wavepacket prepared in the lowest band. Upper panel: time evolution of the weights of the wavepacket on the tight-binding basis orbitals, for tight-binding parameters $\gamma=-U=1$. Lower panel: amplitude A of the Bloch oscillations versus the bandwidth W.

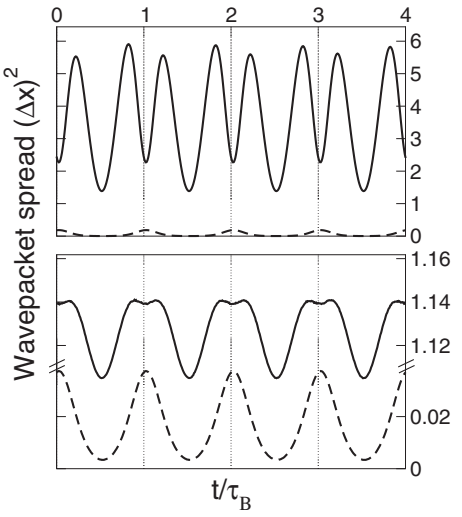

FIG. 3. Time evolution of the total wavepacket spread $(\Delta x)^2$ (solid lines) and of the metric contribution $\langle G_k\rangle$ (dashed lines), for two different sets of tight-binding parameters. Upper panel: $\gamma=-U=1$, resulting in a bandwidth $W\sim0.5$ and a minimum band gap $E_g^{(0)}\sim1.1$. Lower panel: $\gamma=0.5$ and $U=-1$, for which $W\sim0.1$ and $E_g^{(0)}\sim1.2$.

Next we analyze the behavior of the wavepacket spread in the course of the Bloch oscillations, by tracking each of the three terms in Eq. (20). According to Eq. (6), as the center $\langle k\rangle$ of the packet traverses the Brillouin zone, the shape of the wave form f_k remains unchanged. Hence the term $(2\pi/a)\int dk(\partial_k f_k)^2$ is a constant of motion. Oscillations in the spread must therefore arise from the other two terms $\langle G\rangle$ and $\langle(\Delta A)^2\rangle$ (henceforth the k subscript will be omitted for brevity).

Since initially the wavepacket was minimal $[\langle(\Delta A)^2\rangle=0]$, one might have expected spread oscillations to arise mostly from the k-space dispersion of the metric, i.e., from the varying constraint imposed by the uncertainty relation (25) as the wavepacket moves through k space. Instead we find that after an initial transient the spread of the packet can become far from minimal, with $\overline{\langle(\Delta A)^2\rangle}\gg\overline{\langle G\rangle}$ (the bars denote a time average over several Bloch oscillations). This is the situation depicted in the upper panel of Fig. 3, which pertains to the same simulation run as in the upper panel of Fig. 2. Note that the spread undergoes sizable oscillations, arising mostly from $\langle(\Delta A)^2\rangle$ (not shown).

The above scenario is typical of Bloch oscillations in a relatively wide band. When we adjust the tight-binding parameters so as to reduce the bandwidth, we find that the wavepacket remains close to minimal in the course of the Bloch oscillations and the associated spread oscillations are very weak, of the order of the Brillouin-zone dispersion of the metric (lower panel of Fig. 3). One could try to enhance

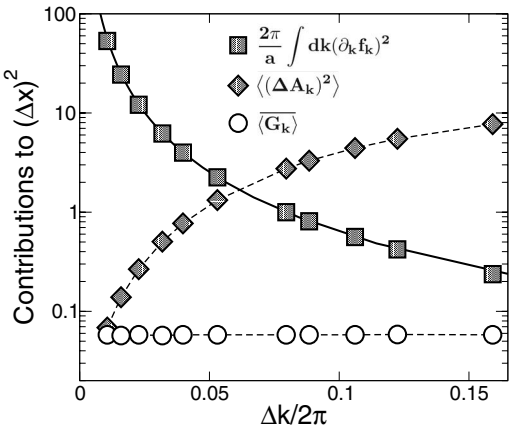

FIG. 4. Dependence of the time-averaged contributions to the wavepacket spread [Eq. (20)] on the wave form width Δk, for $\gamma=-U=1$. The two dashed lines are fits to the values from the numerical simulation (symbols), while the solid line equals the right-hand side of Eq. (27).

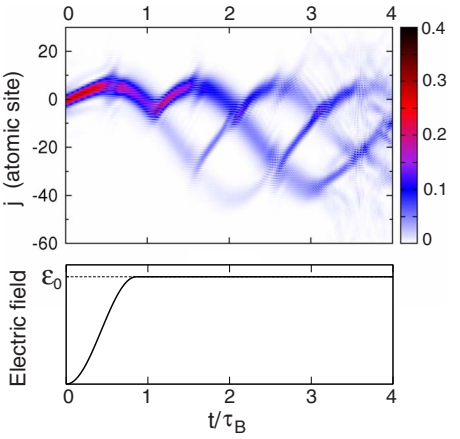

FIG. 5. (Color online) Upper panel: time evolution of a wavepacket prepared in the lowest band, with child packets in the second and third bands appearing as a result of Zener tunneling. The tight-binding parameters are $\gamma=1$ and $U=-0.3$. Lower panel: electric field as a function of time. The field is switched on from $t=0$ to $t=0.86\tau_B$, where τ_B is the Bloch period for the saturation field $\mathcal{E}_0$.

the spread oscillations by further tuning the model parameters so as to make the metric very large in some regions of k space. However, that would require very small gaps and under those circumstances the Bloch oscillations are strongly damped by Zener tunneling.

So far we have considered a fixed waveform width $\Delta k=0.075\times 2\pi$. Figure 4 displays the dependence on Δk of each contributions to $(\Delta x)^2$ averaged over several Bloch oscillations. The term $\overline{\langle G\rangle}$ is roughly constant and equal to the Brillouin-zone average of the metric; it remains a small fraction of $(\Delta x)^2$ over the entire range of Δk. For $\Delta k \ll 2\pi/a$ the spread is dominated by the term $(2\pi/a)\int dk(\partial_k f_k)^2$, while for larger values of Δk the term $\overline{\langle(\Delta A)^2\rangle}$ takes over. Its monotonic increase is easily understood: the larger the range Δk, the larger the spread of A_k over that range is likely to be.

C. Zener tunneling in a strong electric field

In Sec. IV B a weak electric field ($\mathcal{E}_0 \ll E_g^{(0)}/a$) was chosen, so that for the duration of the simulation the wavepacket remained mostly in the lowest band. For sufficiently strong fields, significant interband transitions are expected to occur as the wavepacket reaches the zone center, where the gap is smallest. In order to observe this phenomenon the saturation field was increased from $\mathcal{E}_0=0.055$ to $\mathcal{E}_0=0.09$, while the minimum gap between the first two bands was reduced from $E_g^{(0)}=1.14$ to $E_g^{(0)}=0.31$ by setting $U=-0.3$. With this choice of parameters, a very good stability of the propagation algorithm is needed and we decreased the time step from 2×10^{-3} to 2×10^{-4}. The Brillouin zone was sampled over 300 k points.

The Zener tunneling can be seen in the upper panel of Fig. 5 as a splitting of the wavepacket in real space. At the end of every Bloch oscillation, $t=n\tau_B$ ($n=1,2,\ldots$), the main wavepacket in the lowest band spawns child packets which oscillate in the second band with the same period τ_B but a larger amplitude (due to the larger width of the second band) and gain more weight after each Bloch cycle. These child packets also spawn grandchild packets at $t=(2n+1)\tau_B/2$, when Zener tunneling from the second to the third band becomes possible.

A more quantitative picture is obtained by monitoring the distribution of the packet among the three bands. We define the band occupancy $P_n(t)$ as the total probability that the wavepacket resides on band n (Ref. 10),

$$P_n(t)=\sum_k f_k^2(t)|\langle u_{nk}^{(0)}|v_k(t)\rangle|^2. \tag{30}$$

This quantity is plotted in Fig. 6 as a function of time. Initially only the first band is occupied. After a Bloch period, the wavepacket reaches the zone center, where the gap to the second band is smallest, at which point significant Zener tunneling occurs, giving rise to a partial occupation of the second band. (Between $t=0$ and $t=\tau_B$ the wavepacket moved in k space by less than the full Brillouin-zone width, from $\langle k\rangle=-2\pi/3$ to $\langle k\rangle\simeq -2\pi$, because during most of that time interval the electric-field strength was less than $\mathcal{E}_0$, as shown in the lower panel of Fig. 5.) Subsequently there are also

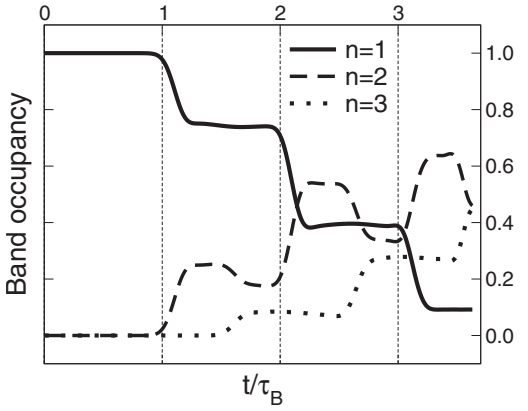

FIG. 6. Band occupancy $P_n(t)$ for the simulation shown in Fig. 5.

transitions to the third band, again with periodicity τ_B; because transitions from the second band to the first and third bands happen at the zone center and at the zone boundary, respectively, P_2 undergoes changes twice as often as P_1 and P_3.

V. CONCLUSIONS

In this work we have developed a numerical scheme for simulating wavepacket dynamics in a periodic lattice potential with a linear potential (homogeneous electric field) superimposed. By using the k-space representation of the position operator, we were able to include the linear electric-field term $e\mathcal{E}\cdot\mathbf{r}$ in the Hamiltonian under periodic boundary conditions, thus avoiding having to use large supercells with hard-wall boundary conditions.[10]

In the present approach, the wavepacket is represented on a uniform mesh of k points by a wave form f_k sitting on top of a "band" of states $|v_k\rangle$ [Eq. (1)]. The time evolution of the wavepacket is then obtained from that of f_k and $|v_k\rangle$. For $\mathcal{E}\neq 0$ the states $|v_k\rangle$ become nonadiabatic, field-polarized Bloch states which span several energy bands of the field-free crystal Hamiltonian H^0 (a similar representation of wavepackets in coupled energy bands was used in Ref. 22); thus interband effects, such as Zener tunneling, are fully accounted for.

The method was tested on a one-dimensional tight-binding model. Depending on the choice of tight-binding parameters and electric-field strength, we observed either long-lived Bloch oscillations or short-lived Bloch oscillations strongly damped by Zener tunneling. In the former regime, we monitored the changes in the wavepacket spread accompanying the Bloch oscillations of the center of mass and identified two distinct situations. (i) For wavepackets moving in narrow bands, the spread changed very little over time. (ii) For wavepackets moving in wide bands, the Bloch oscillations were accompanied by considerable oscillations of the wavepacket spread. An analysis of the k-space expression for the spread [Eq. (20)] reveals two distinct contributions which can change over time: one associated with the Berry connection of the underlying Bloch states and another related to the quantum metric. By tracking each of them separately, we concluded that in the cases where significant spread oscillations took place, they originated mostly in the Berry connection term.

ACKNOWLEDGMENTS

We thank David Vanderbilt for useful discussions. This work was supported by the Marie Curie OIF program of the EU and by the NSF under Grant No. DMR-0706493.

APPENDIX: DISCRETIZED EXPRESSIONS IN k SPACE

Here we derive the discretized versions used in Sec. IV of the dynamical equations of Sec. II and of the wavepacket center and spread expressions of Sec. III.

1. Dynamical equations

The appropriate finite-difference representation of $|\tilde{\partial}_k v_k'\rangle$ on a uniform grid is[13]

$$|\tilde{\partial}_k v_k'\rangle = \frac{1}{2b}(|\tilde{v}_{k+b}\rangle - |\tilde{v}_{k-b}\rangle), \tag{A1}$$

where b is the mesh spacing and

$$|\tilde{v}_{k+b}\rangle = \frac{|v_{k+b}'\rangle}{\langle v_k'|v_{k+b}'\rangle}. \tag{A2}$$

We use Eq. (A1) to recast Eq. (8) as[13]

$$i|\dot{v}_k'\rangle = T_k|v_k'\rangle, \tag{A3}$$

in terms of the Hermitian operator,

$$T_k = H_k^0 + w_k + w_k^\dagger, \tag{A4}$$

where $w_k=(i\mathcal{E}/2b)(P_k^+-P_k^-)$ and $P_k^\pm=|\tilde{v}_{k\pm b}\rangle\langle v_k'|$. Equation (A3) is solved numerically at each grid point using[10,13]

$$|v_k'\rangle(t+\Delta t) \simeq \frac{1-i(\Delta t/2)T_k(t)}{1+i(\Delta t/2)T_k(t)}|v_k'\rangle(t). \tag{A5}$$

Because of the similarity between Eqs. (10) and (A3), the phase factors U_k can be propagated in time using the same algorithm. A finite-difference representation for the connection in Eq. (10) is needed. We use[18]

$$A_k \simeq -\frac{1}{2b}(\Phi_k^+ - \Phi_k^-), \tag{A6}$$

where we have defined the phases $\Phi_k^\pm=-\mathrm{Im}\ \ln\langle v_k|v_{k\pm b}\rangle$. When propagating U_k via Eq. (10), care must be taken in choosing consistently the branch cuts for the two phases in Eq. (A6) to ensure that A_k remains a smooth function of k at every time step.

2. Wavepacket center and spread

In order to obtain a finite-difference representation of Eq. (15), we make the replacement $\int dk\to\Sigma_k b$ and then use Eq. (A6). A few manipulations yield

$$\langle x\rangle \simeq -\frac{2\pi}{a}\sum_k \frac{1}{2}(f_k^2+f_{k+b}^2)\Phi_k^+. \tag{A7}$$

To find an expression for $(\Delta x)^2$ we start from Eq. (20). The first term on the RHS is easily discretized and $\langle G_k\rangle$ can be evaluated from Eq. (21). The remaining term is $\langle A_k^2\rangle-\langle A_k\rangle^2$. For $\langle A_k\rangle^2=\langle x\rangle^2$ we use Eq. (A7) and, from Eq. (A6),

$$\langle A_k^2\rangle \simeq \frac{\pi}{b}\sum_k\left[\frac{f_k^2+f_{k+b}^2}{2}(\Phi_k^+)^2 - f_k^2\Phi_k^+\Phi_k^-\right]. \tag{A8}$$

Besides reducing to the correct continuum expressions as $b\to 0$, Eqs. (A7) and (A8) preserve exactly, for finite b, certain properties of those expressions. If we perform a change in phases

$$|v_k\rangle \to e^{i\theta_k}|v_k\rangle \tag{A9}$$

with $\theta_k=\gamma_k-kR$ (R is a lattice vector and $\gamma_{k+2\pi/a}=\gamma_k$), the center of the packet (15) changes as

$$\langle x\rangle \to \langle x\rangle + R - \frac{2\pi}{a}\int dk\ f_k^2 \partial_k \gamma_k. \tag{A10}$$

For a Wannier wavepacket f_k is constant, so that the last term vanishes, and $\langle x\rangle$ changes at most by a lattice vector.[19] If instead f_k spans a narrow region $\mathcal{K}$ of the Brillouin zone, $\langle x\rangle$ can then shift continuously under Eq. (A9). Consider the choice

$$\theta_k = \begin{cases} -\delta k & k \in \mathcal{K} \\ 0 & \text{otherwise}, \end{cases} \tag{A11}$$

which produces a rigid shift $\langle x\rangle \to \langle x\rangle + \delta$. Equation (A7) obeys this transformation exactly, while the spread evaluated using Eq. (A8) remains unchanged, as can be easily verified.

[1] J. Feldmann, K. Leo, J. Shah, D. A. B. Miller, J. E. Cunningham, T. Meier, G. von Plessen, A. Schulze, P. Thomas, and S. Schmitt-Rink, Phys. Rev. B **46**, 7252 (1992).

[2] M. Ben Dahan, E. Peik, J. Reichel, Y. Castin, and C. Salomon, Phys. Rev. Lett. **76**, 4508 (1996).

[3] T. Pertsch, P. Dannberg, W. Elflein, A. Bräuer, and F. Lederer, Phys. Rev. Lett. **83**, 4752 (1999).

[4] R. Sapienza, P. Costantino, D. Wiersma, M. Ghulinyan, C. J. Oton, and L. Pavesi, Phys. Rev. Lett. **91**, 263902 (2003).

[5] O. Morsch, J. H. Müller, M. Cristiani, D. Ciampini, and E. Arimondo, Phys. Rev. Lett. **87**, 140402 (2001).

[6] Q. Niu, X.-G. Zhao, G. A. Georgakis, and M. G. Raizen, Phys. Rev. Lett. **76**, 4504 (1996).

[7] H. Trompeter, T. Pertsch, F. Lederer, D. Michaelis, U. Streppel, A. Brauer, and U. Peschel, Phys. Rev. Lett. **96**, 023901 (2006).

[8] M. Cristiani, O. Morsch, J. H. Müller, D. Ciampini, and E. Arimondo, Phys. Rev. A **65**, 063612 (2002).

[9] M.-C. Chang and Q. Niu, J. Phys.: Condens. Matter **20**, 193202 (2008).

[10] A. M. Bouchard and M. Luban, Phys. Rev. B **52**, 5105 (1995).

[11] I. Souza, J. Íñiguez, and D. Vanderbilt, Phys. Rev. Lett. **89**, 117602 (2002).

[12] P. Umari and A. Pasquarello, Phys. Rev. Lett. **89**, 157602 (2002).

[13] I. Souza, J. Íñiguez, and D. Vanderbilt, Phys. Rev. B **69**, 085106 (2004).

[14] E. N. Blount, Solid State Phys. **12**, 305 (1962).

[15] J. Callaway, *Quantum Theory of the Solid State: Part B* (Academic, New York, 1974).

[16] C. Kittel, *Introduction to Solid State Physics*, 8th ed. (Wiley, New York, 2005).

[17] See Eq. (6.1.9) of Ref. 15. Note that the quantity $\phi_n(k)$ therein, the CMR expansion coefficient of the wavepacket, is given in our notation by $f_k c_{nk}$, so that $\Sigma_n|\phi_n(k)|^2 = f_k^2 \Sigma_n |c_{nk}|^2 = f_k^2$.

[18] N. Marzari and D. Vanderbilt, Phys. Rev. B **56**, 12847 (1997).

[19] R. D. King-Smith and D. Vanderbilt, Phys. Rev. B **47**, 1651 (1993).

[20] In practice a constant A_k can be achieved on a uniform mesh following the prescription in Sec. III.C.1 of Ref. 18.

[21] I. Souza, T. Wilkens, and R. M. Martin, Phys. Rev. B **62**, 1666 (2000).

[22] D. Culcer, Y. Yao, and Q. Niu, Phys. Rev. B **72**, 085110 (2005).